V European Conference on Computational Fluid Dynamics
ECCOMAS CFD 2010
J. C. F. Pereira and A. Sequeira (Eds)
Lisbon, Portugal, 14–17 June 2010

CFD ANALYSIS OF CREEPING FLOW AROUND A SPHERICAL PARTICLE IN RECTANGULAR MICROCHANNELS

José L.C. Santos[*†], Luís P. Fonseca [††], Vítor Geraldes[†††]

[†]Requimte/CQFB, Departamento de Química, Faculdade de Ciências e Tecnologia,
Universidade Nova de Lisboa
Campus de Caparica, 2829-516 Caparica, Portugal
jose.santos@dq.fct.unl.pt
[††]Centro de Engenharia Biológica e Química, Instituto Superior Técnico, Av. Rovisco Pais,
1049-001 Lisboa, PORTUGAL
e-mail: luis.fonseca@ist.utl.pt
[†††]ICEMS, Departamento de Engenharia Química e Biológica, Instituto Superior Técnico,
Universidade Técnica de Lisboa
Av. Rovisco Pais 1, 1049-001 Lisboa, Portugal
vitor.geraldes@ist.utl.pt

Key words: Microfluidics, Fluid Dynamics

Abstract. *The laminar flow of Newtonian fluids with suspended small particles in rectangular narrow channels has been receiving increasing attention owing to development of micro-devices for biomedical and micro-chemical technologies. The objective of the present study is to investigate the effect of the narrow rectangular channel height, sphere diameter and position on the drag force and torque that the fluid exerts on a sphere at rest or moving with uniform linear or uniform angular velocity, near the microchannel walls. Numerical simulations of creeping flow were performed by using the OpenFOAM 1.5 CFD software package, where the pressure-velocity coupling was managed by the SIMPLE algorithm. All the discretization schemes used in the CFD calculations were fourth order accurate, and the linear solvers tolerance were fixed at 10^{-7}. The computational mesh was generated by the snappyHexMesh utility, with a larger refinement level near the sphere surface. A total of 1020 CFD simulations were carried out in a 254 CPU computational cluster with an average simulation time of 6 hours per simulation. The ratio between the sphere diameter and channel height was varied between 0.05 and 0.8. The results showed that for sphere diameters of the same order of the channel height the calculated drag force strongly deviates from the Stokes force. The deviation is particularly high when the sphere touches the channel wall or when its radius is high. The torque exerted by the fluid on the spherical particle increases both with the particle radius and with the proximity to the channel walls. When the particle is moving and rotating in contact with the wall, it was observed that there is not a simultaneous equilibrium point both for the drag force and torque, and, therefore, a free-moving sphere near the channel walls must slip and rotate at the same time.*

1 INTRODUCTION

The laminar flow of Newtonian fluids with suspended small particles in narrow channels has gained in the last years considerable importance with the fast-growing development of micro-devices for biomedical and micro-chemical technologies [e.g. 1,2]. In particular, the design of microfluidic micro-total-analytical-systems, which are based on the separation of magnetic microspheres from the fluid by using magnetic fields [3], may be facilitated with prediction methods of drag force and torque exerted on the particle by fluid.

In these systems the dimensions of the particles are often of the same order of magnitude of the channels height and, for this reason, the particles can not be regarded as a point mass and expedite Lagrangian particle tracking numerical methods fail too predict the movement of the particles (and the forces acting on them by the fluid) inside the channels, after the computation of the fluid velocity distribution [3]. Some authors suggest, without experimental or theoretical evidence, that Lagrangian particle tracking methods can still be used in micro devices, without specifying the limits of this approach [e.g. 4]. Yet, for particles with a diameter one order-of-magnitude lower than the microchannel height, the Stokes equation seems adequate to compute the drag force [5,6].

When the size of the suspended particles is of the same order of magnitude of the channel thickness, more detailed work using computational fluid dynamics tools [7] has shown that the flow structure is influenced by the presence of the particle. In this situation, the torque, and drag and lift forces acting on the particle by the fluid cannot be computed by assuming that domain is unbounded and the velocity profiles are linear. Hence, in these circumstances and for a spherical particle, the Saffman's lift force equation [8] and the Stokes law for the drag force are no longer valid.

The prediction of the laminar flow of Newtonian fluids with suspended small particles in narrow channels by computational fluid dynamics (CFD) is a valuable tool for predicting the drag force and torque acting on the particle. For a single rigid particle, with a given geometry, flowing with the fluid inside the channel, the more rigorous numerical method to compute the fluid velocity distribution and the particle movement is to solve the Navier-Stokes equation by CFD using a dynamic mesh around the moving particle, which has 6 degrees of freedom. As this approach is computationally expensive, when the particle is at rest or moving with uniform linear or angular velocity, it is still possible, by a fraction of the computation cost of the more rigorous approach, to obtain useful information by CFD using a fixed grid. In this case, information about the drag force or torque is obtained that is very useful to establish the optimal conditions for the separation of magnetic particles, for instance.

The purpose of this paper is to investigate the effect of channel height, sphere diameter and vertical position on the drag force and torque that the fluid exerts on a sphere at rest or moving with uniform linear or uniform angular velocity, near the microchannel walls. In addition the conditions of validity of the Stokes equation for this system are presented.

2 PHYSICAL SYSTEM

The physical system studied in this work is depicted in Figure 1. A Newtonian fluid with a viscosity μ and a density ρ enters in the narrow rectangular channel with a parabolic velocity profile, with a maximum velocity U_0. A sphere with a radius R_P, is located inside the channel at a distance y_P from the centered horizontal plane and moves

with the fluid with a U_P linear velocity and with a ω_P angular velocity. Under these conditions, the sphere is subjected to a horizontal drag force F_D, a vertical lift force F_L, and a moment force F_M, perpendicular to the xy plane.

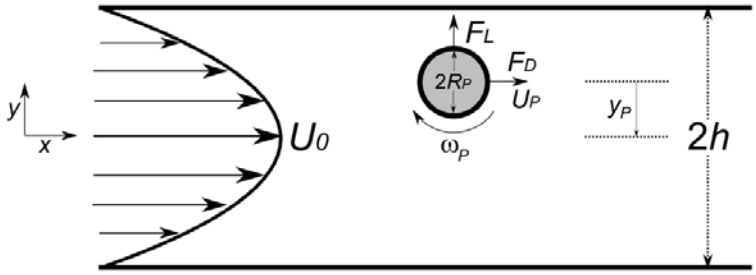

Figure 1: Physical system under study and forces acting on the sphere.

2.1 Governing Equations and Numerical Method

For very low Reynolds numbers, the flow is considered to be solely governed by viscous effects, being commonly described as Stokes flow or creeping flow [9]. In these conditions, the mass continuity and Navier-Stokes equations are given by:

$$\nabla \cdot \mathbf{U} = 0 \tag{1}$$

$$\nabla \cdot \left(\nu \nabla \mathbf{U}\right) = \nabla p \tag{2}$$

where **U** is the fluid velocity vector, ν is the kinematic viscosity of the fluid, and p is the kinematic pressure.

The numerical simulations were performed by using the OpenFOAM 1.5 CFD software package [10], which is composed by a set of open-source libraries, allowing for an expedite development of tailored solvers and applications. OpenFOAM is based on the finite-volume method [11] with a collocated variable arrangement. The pressure-velocity coupling in the solution of Eqs. 1 and 2 was managed by the SIMPLE algorithm [12].

Computational Domain and Boundary Conditions. To reduce the volume of the computational domain, a referential moving with the spherical particle was used. In this referential, the channel walls are moving backward with a negative velocity U_P. With this approach it was possible to use a domain with an height of $2h$, a length of $8h$ and a width of $8h$. In order to reduce further the computational load, a symmetry plane was defined at the plane $z = 0$. Therefore, the computational domain comprises only half of the channel, as shown in Figure 2. An additional symmetry plane was defined for $z = 4h$, while a no-slip boundary condition was imposed on the top and bottom walls. The linear velocity on the surface of the spherical particle was imposed taking into account its angular velocity. At the channel outlet, a zero velocity gradient was imposed.

Mesh generation. The computational mesh used for the numerical simulations was generated using the snappyHexMesh OpenFOAM utility. The snappyHexMesh utility automatically generates a high-quality mesh comprised mostly by hexahedra. The meshing process starts from a hexahedral background mesh, and iteratively adapts to the sphere surface. Larger cell refinement levels were defined for the sphere surface. The

last step of the meshing process introduced a pre-defined number of layers of hexahedral cells in the boundary layer close to the sphere surface.

The resulting mesh for the larger R_P^* value of 0.8, shown in Fig. 3, was obtained after a grid-independence study, where the drag force and shear stress at the sphere surface were used as monitoring quantities between meshes of different refinement levels. This mesh has 1.4 million cells, with a larger cell density in the vicinity of the sphere. The cell density of this mesh was maintained in the generation of the meshes for the remaining R_P^* values.

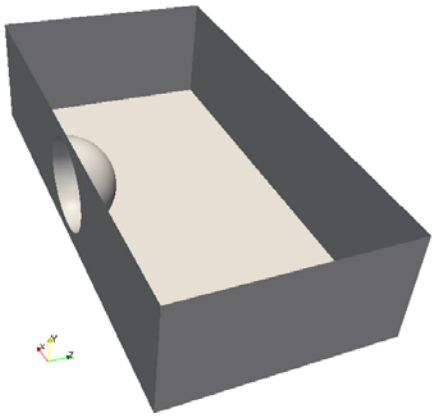

Figure 2: Computational domain, with symmetry planes defined for z =4h and z = 0.

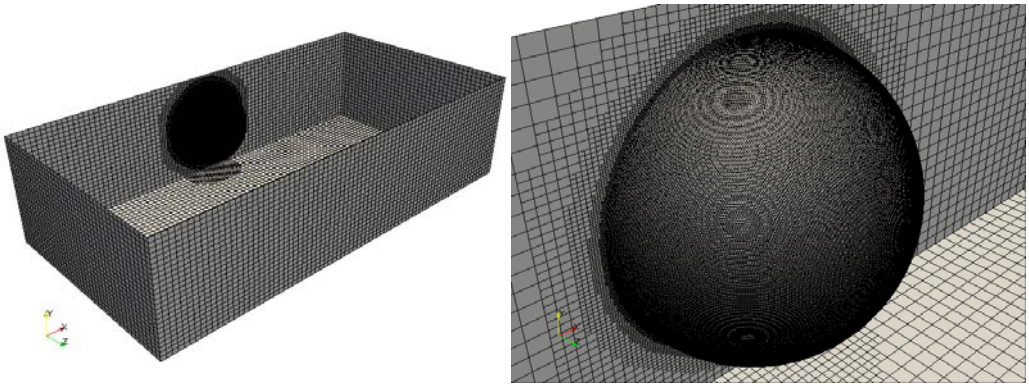

Figure 3 – Surface detail of the computational mesh with 1.4 million cells used in the CFD simulations for a R_P^* of 0.8.

2.2 Discretization schemes and solution control

All the discretization schemes used in the CFD calculations were fourth order accurate. The linear solvers used in this work were the Geometric Agglomerated algebraic MultiGrid solver (GAMG) solver for the pressure with a relative tolerance of 0.01 and an absolute tolerance of 10^{-7}, and the Preconditioned Conjugate Gradient (PCG) solver for the velocity with a relative tolerance of 0.1 and an absolute tolerance of 10^{-7}. Under-relaxation coefficients of 0.3 and 0.7 were selected for pressure and velocity, respectively. Three non-orthogonal correctors were used in order to cope with the non-orthogonality in the mesh near the sphere surface. This means that the pressure correction step in the SIMPLE algorithm is run 3 times. Full solution convergence was

always achieved with about 2000 iterations, meaning that the absolute residual tolerances of pressure and velocity were met.

The CFD simulations were carried out in a 254 CPU computational cluster (AMD Opteron cluster with 2.8 GHz CPU's and 1 GB RAM/CPU), with an average simulation time of 6 hours per simulation. The computational meshes were decomposed for parallel processing in order to maintain a ratio of 100 thousand cells/CPU.

2.3 Dimensional analysis

The drag force, F_D, and the resulting moment of force (torque), T, that the fluid in the rectangular microchannel exerts on a sphere moving with a uniform linear velocity U_P and with a uniform angular velocity ω may be put on a dimensionless form as follows:

$$\Pi_D \equiv \frac{F_D}{\mu h U_0} \tag{3}$$

$$\Pi_T \equiv \frac{T}{\mu h^2 U_0} \tag{4}$$

A dimensional analysis reveals that the previous independent dimensionless numbers are function of the following dimensionless numbers

$$y_p^* = y_p /(h - R_P) \tag{5}$$

$$R_P{}^* = R_P / h \tag{6}$$

$$\omega^* = \omega R_P / U_0 \tag{7}$$

$$U_P{}^* = U_P / U_0 \tag{8}$$

2.4 Parametric set-up of the CFD simulations.

A parametric CFD study was performed by varying the independent dimensionless numbers in a wide range of values, as shown in Table 1.

Table 1 – Range of independent dimensionless numbers in the parametric CFD study.

$R_P{}^*$	0.05, 0.1, 0.2, 0.35, 0.5, 0.8
$y_P{}^*$	0, 0.25, 0.5, 0.75, 1
$U_P{}^*$	0, 0.01, 0.03, 0.1, 0.3, 0.9, 1
ω^*	0, 0.1, 0.2, 0.5, 0.75, 1

3 RESULTS AND DISCUSSION

The vector distribution of the velocity in the center plane *xy* and the distribution of shear stress magnitude at the spherical particle surface is displayed in Fig. 4, for $R_P{}^* = 0.5$, $U_P{}^* = 0$, and $y_p{}^* = 1$. As shown in this figure, the density of nodes that was

used is more than sufficient to resolve with accuracy the velocity field. In this particular case, as the diameter of the particle is half of the channel height, the velocity field in the center of the channel is strongly affected by the presence of the particle.

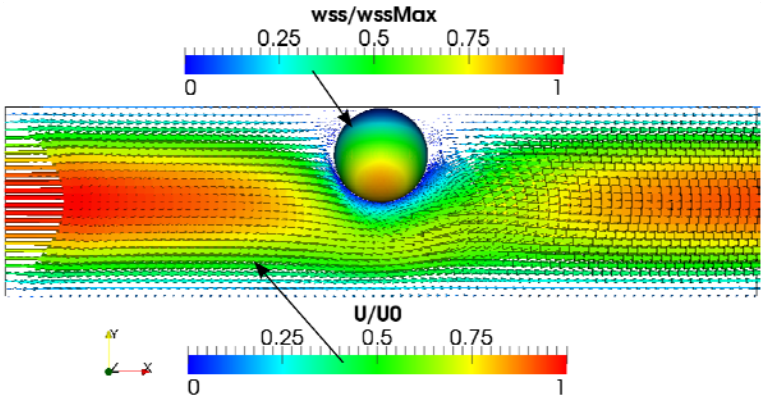

Figure 4: Vector distribution of the velocity in the center plane *xy* and distribution of shear stress magnitude at the spherical particle surface (R_P^* = 0.5, U_P^* = 0, y^* = 1).

For a motionless sphere, the ratio between the drag force and the Stokes force, computed with the inlet U_y value at the same level of the sphere center, is higher than 1 and is a function of R_P* and y_P* (Fig. 5). This ratio is particular high when the sphere touches the channel wall or when its radius is high. When the sphere touches the wall, the following correlation fits the numerical predictions with a maximum relative error of 0.4%

$$\frac{F_D}{F_{Stokes}} = 1 + 1.33(y_p^*)^{2.4} + 0.62(y_p^*)^{0.13} \tag{10}$$

For the motionless sphere in the center of the channel (y^*_p = 0), the following correlation fits the CFD predictions with a maximum relative error less than 1.6%.

$$\frac{F_D}{F_{Stokes}} = 1 + 1.9(y_p^*)^{1.5} \tag{11}$$

The dimensionless torque number Π_T, also for the motionless sphere, increases both with y^*_{p} and with R^*_p and is zero when the sphere is located in the middle of the channel at y^*_p = 0, as expected (Figure 6). Between $0.05 \le R^*_P \le 0.5$ the correlation

$$\Pi_T = 11.6(y_p^*)^{0.9}(R_p^*)^2[1 - 0.9R_p^*] \tag{12}$$

fits the CFD prediction with a maximum error less than 5%.

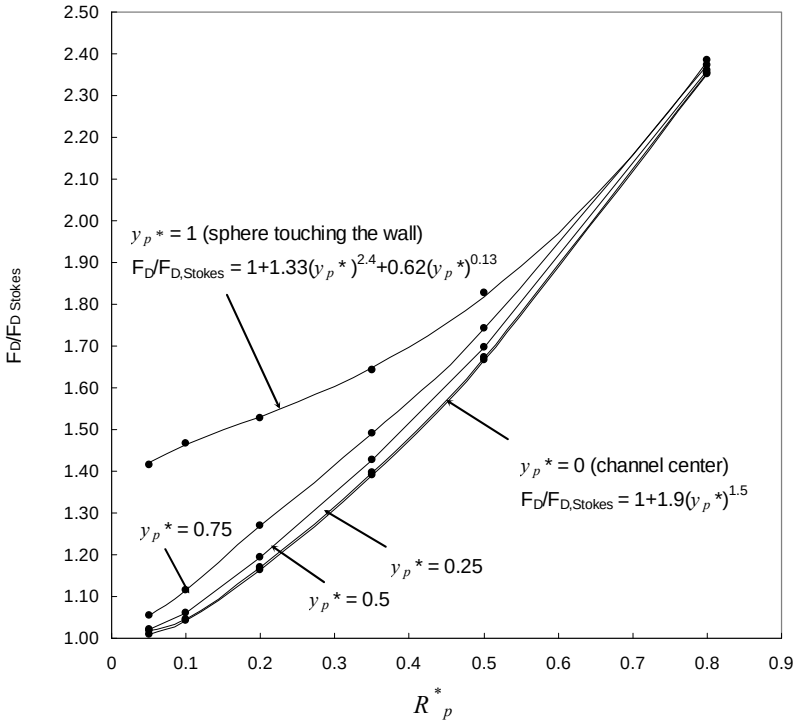

Figure 5: Ratio $F_D/F_{DStokes}$ vs. R_P^* for different values of y_P^*. and for a motionless spherical particle.

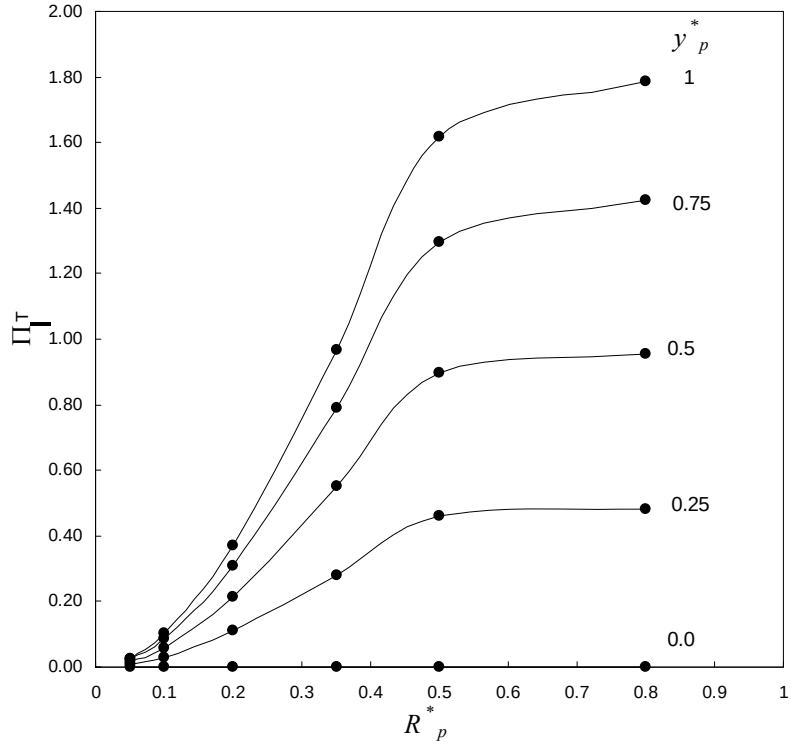

Figure 6: Dimensionless torque number Π_T, vs. R_P^* for different values of y_P^*, and for a motionless spherical particle.

When the particle rotates in contact with the channel without slipping ($U_P = \omega R_P$), both the dimensionless drag force and torque increase with the angular velocity and depend on the sphere radius (see Figure 7 and 8).

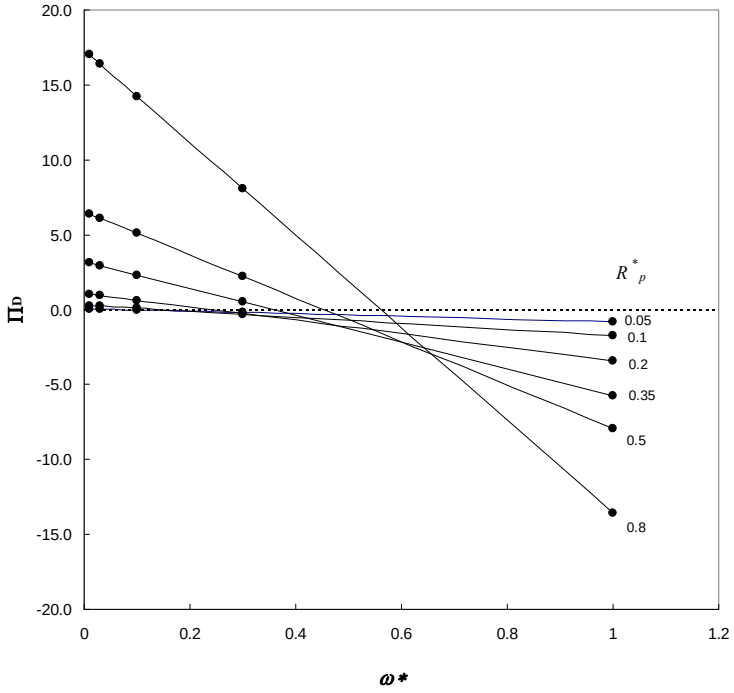

Figure 7: Dimensionless drag force Π_D, vs. ω^* for different values of R_P^* and for a non-slipping spherical particle rotating over the channel wall.

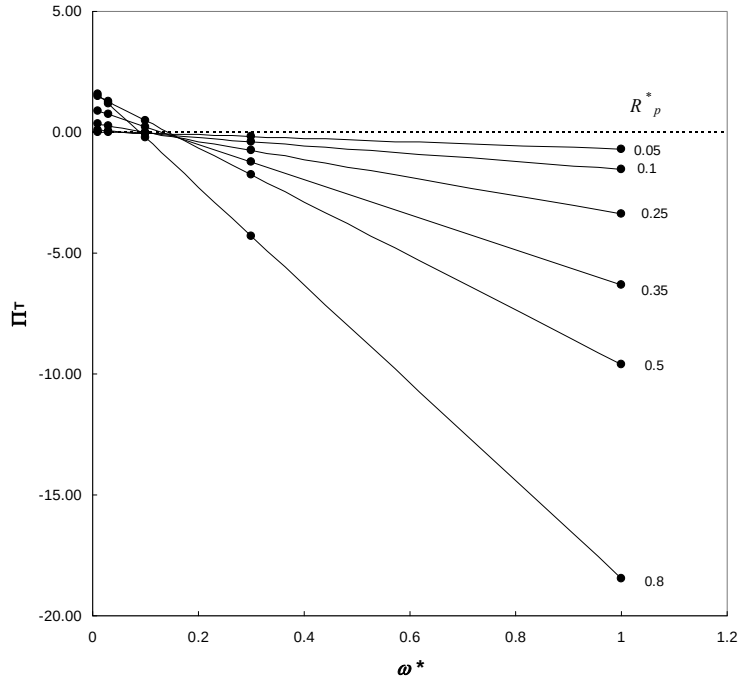

Figure 8. Dimensionless torque Π_T, vs. ω^* for different values of R_P^* and for a non-slipping spherical particle rotating over the channel wall.

There is a critical value of the dimensionless angular velocity for which the drag force is zero and this value depends on the dimensionless sphere radius, as seen in Fig. 7. This critical value can also be defined based on the condition of zero torque (see Fig. 8). These critical dimensionless angular velocities vs. R^*_p are displayed in Figure 9. The analysis of this figure shows that the two critical velocities are never equal and, hence, when the sphere rotates on the wall without slipping the drag force and torque

can never be both zero. This means that, for this condition of the sphere movement, there is not an equilibrium point. Therefore, a freely-moving sphere must slip and rotate at the same time when it moves on the top of the wall. The angular velocity of the spherical particle must be within the dashed region of Fig. 9.

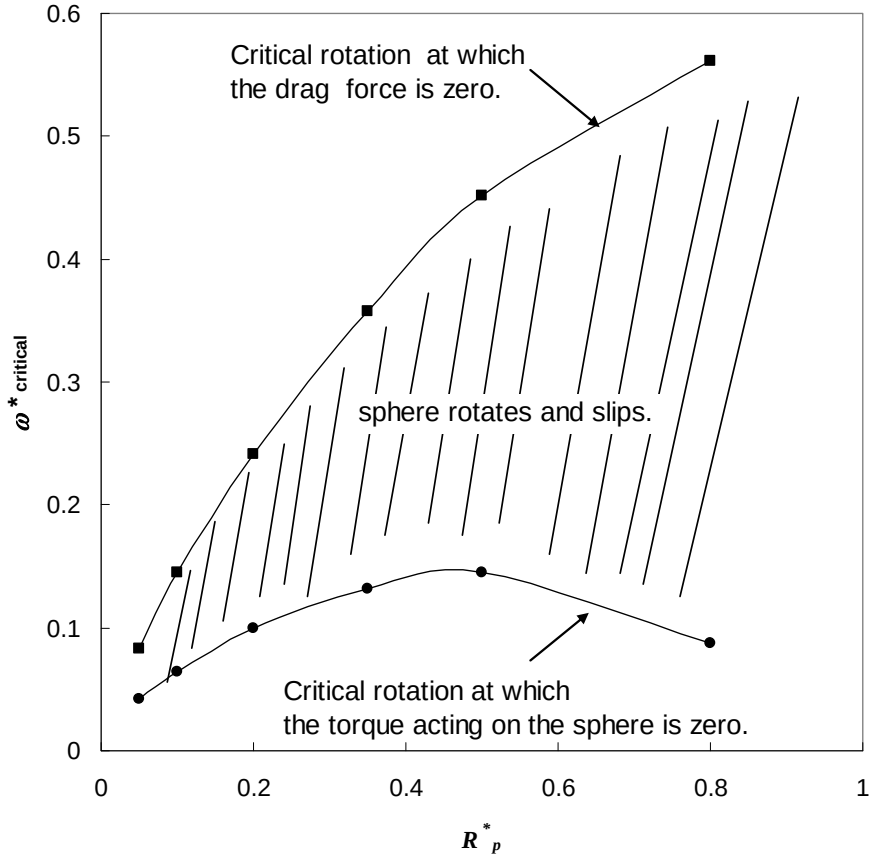

Figure 9. Critical values of ω^* vs. R_P^* for a non-slipping spherical particle rotating over the channel wall.

4. CONCLUSIONS

A numerical analysis using the OpenFOAM 1.5 CFD software package was performed to investigate the movement of a spherical particle inside a narrow rectangular channel with a Newtonian fluid in laminar creeping flow, assuming that the sphere was either at rest or moving with uniform linear or angular velocity adjacent to the narrow rectangular microchannel walls. The results have shown that for sphere diameters of the same order of the channel height the calculated drag force strongly deviates from the Stokes equation. The deviation is particularly high when the sphere touches the channel wall or when its radius is high. The torque exerted by the fluid on the spherical particle increases both with the particle radius and with the proximity to the channel walls. When the particle is moving in contact with the channel walls, it was observed that there is not an equilibrium point of drag force and torque, and sphere that moves freely in the circulating fluid must slip and rotate at the same time. Several correlations for the dimensionless drag force and torque numbers were derived that can be useful to identify equilibrium force conditions that prevail when, for instance, external magnetic forces act on the particle.

AKNOWLEDGEMENTS

The authors Vitor Geraldes and Luis P. Fonseca would like to acknowledge FCT for the financial support to the project: PTDC/AMB/73154/2006 (SpinAquaChip).

REFERENCES

[1] Nilsson J , Evander M , Hammarstrom B, Laurell T, Review of cell and particle trapping in microfluidic systems, *Analytica Chimica Acta*, **649(2),** pp 141-157 (2009)

[2] Das T, Chakraborty S , Biomicrofluidics: Recent trends and future challenges, *Sadhana-Academy Proceedings in Engineering Sciences* , **34(4)**, pp. 573-590 (2009)

[3] Shinichi Ookawara , Madhusuden Agrawal , David Street, Kohei Ogawa, Quasi-direct numerical simulation of lift force-induced particle separation in a curved microchannel by use of a macroscopic particle mode, *Chem. Eng. Sci.,* **62** pp. 2454 – 2465 (2007)

[4] Yonghao Zhang, Robert W. Barber and David R. Emerson, Particle Separation in Microfluidic Devices - SPLITT Fractionation and Microfluidics, *Current Analytical Chemistry* **1**, pp. 345-354 (2005)

[5] A. Sinha, R. Ganguly, A. K. De and I.K. Puria, Single magnetic particle dynamics in a microchannel, *Physics of Fluids* **19**, pp. 117102 (2007)

[6] E. P. Furlani, Y. Sahoo, K. C. Ng, J. C. Wortman, T. E. Monk, A model for predicting magnetic particle capture in a microfluidic bioseparator, *Biomed. Microdevices* **9**, pp. 451–463 (2007)

[7] Nimisha Shukla and Kimberly H. Henthorn, Effect of relative particle size on large particle detachment from a microchannel, *Microfluid Nanofluid* **6**, pp. 521–527 (2009)

[8] Saffman, P.G., 1965. The lift force on a small sphere in a slow shear flow, *J. Fluid Mech.* **22**, pp. 385–400 (1965)

[9] R.B. Bird, W.E. Stewart and E.N. Lightfoot, Transport Phenomena, *John Wiley & Sons* , New York (1960)

[10] OpenCFD Ltd, OpenFOAM: The Open Source CFD Toolbox. http://www.opencfd.co.uk/openfoam/.

[11] S. Patankar, Numerical Heat Transfer and Fluid Flow, *Taylor & Francis* (1980)

[12] J. Ferziger, M. Peric, Computational Methods for Fluid Dynamics, *Springer*, New York, (1999)